Journal of the Serbian Chemical Society
JSCS-info@shd.org.rs • www.shd.org.rs/JSCS
J. Serb. Chem. Soc. *78* (11) 1689–1702 (2013) UDC 539.216+546.92–3+544.478:66.094.1
JSCS–4527 *Original scientific paper*

Single crystalline thin films as a novel class of electrocatalysts

JOSHUA SNYDER, NENAD M. MARKOVIC and VOJISLAV R. STAMENKOVIC*

Materials Science Division, Argonne National Laboratory, Argonne, IL 60439, USA

(Received 16 September, revised 30 October 2013)

Abstract: The ubiquitous use of single crystal metal electrodes has garnered invaluable insight into the relationship between surface atomic structure and functional electrochemical properties. However, the sensitivity of their electrochemical response to surface orientation and the amount of precious metal required can limit their use. Herein, a generally applicable procedure for the production of thin metal films with a large proportion of atomically flat (111) terraces without the use of an epitaxial template is presented. Thermal annealing in a controlled atmosphere induces long-range ordering of magnetron sputtered thin metal films deposited on an amorphous substrate. The ordering transition in these thin metal films yields characteristic (111) electrochemical signatures using a minimal amount of material and provides an adequate replacement for oriented bulk single crystals. This procedure could be generalized towards a novel class of practical multimetallic thin film-based electrocatalysts with tunable near-surface compositional profiles and morphologies. Annealing of atomically corrugated sputtered thin film Pt-alloy catalysts yields an atomically smooth structure with highly crystalline, (111)-like ordered and Pt segregated surface that displays superior functional properties, bridging the gap between extended/bulk surfaces and nanoscale systems.

Keywords: thin films; magnetron sputtering; Pt-alloys; oxygen reduction reaction.

INTRODUCTION

Well-defined, single crystal metal electrodes and their stepped/vicinal derivatives have helped to elucidate the correlation between surface structure and functional properties for many electrochemical and electrocatalytic processes. Their use has also guided investigations of the mechanistic reaction pathways relevant to hydrogen economy, most notably the oxygen reduction reaction (ORR),[1–4] providing valuable insight into the link between bulk surfaces and nanoscale catalysts,[5–7] To this end, Pt(111)[8] has been the most widely studied single crystal as its close-packed atomic arrangement and wide atomically flat terraces provide an ideal, well-defined surface essentially devoid of defects when

* Corresponding author. E-mail: vrstamenkovic@anl.gov
doi: 10.2298/JSC130916119S

properly prepared. The study of oriented single crystals of single-phase metal alloys has inspired an entire branch of electrocatalyst research and development focused on the optimization of surface interaction with reaction intermediates and products. Most notably, the discovery that annealing a $Pt_3Ni(111)$ single crystal can drive the formation of a segregated compositional profile, where a Pt-skin covering a Ni-rich second atomic layer was found to be the most active surface to date for the ORR.[9]

The wide spread use of high quality single crystal metal electrodes was enabled through the introduction of a technique to reproducibly prepare single crystal bead electrodes by melting, cooling and careful orientation before cutting and polishing to expose the desired crystallographic face.[10–12] Significant care must be taken as even small degrees of miscut can result in significantly altered electrochemical properties due to the increased step density on the surface.[13–16] The cylindrical single crystal geometry is more amenable for use in a rotating disk electrode (RDE) setup for determining the kinetic parameters of electrochemical reactions than the bead type single crystals. These cylindrical single crystals are typically several millimeters in diameter and thickness, requiring a significant amount of material and can only be manufactured in a small number of facilities that have the proper capabilities. As such, cylindrical bulk single crystals are cost prohibitive for general use, especially when composed of precious metals and precious metal containing alloys. Metal thin films present a potential replacement for bulk single crystals as the nature of their geometry both significantly lowers the precious metal content and provides a surface that is susceptible to ordering upon annealing, driven by a tendency to expose the lowest energy surface, the (111) family. The formation of (111) textured thin films is typically achieved through epitaxial growth on single crystal substrates either by slow physical vapor deposition (PVD)[15,17–24] or in solution through electrochemical deposition.[25,26] Films produced in such a manner can be highly strained due to lattice mismatch between the film and substrate and, depending upon the deposition/annealing parameters, the film may contain holes and discontinuities. These PVD films often lack the long-range order required to exhibit cyclic voltammetric (CV) finger-print adsorption features characteristic of (111) single crystals[17,18,26,27] and the few that do have a form factor that is difficult to integrate into an RDE for proper determination of kinetic parameters from electrochemical data.[28,29]

In this report, a simple approach to reproducibly generate well-defined highly ordered (111) surfaces on polycrystalline thin metal films without the use of epitaxial templates or seeded layer growth is presented. The processing of these magnetron sputtered polycrystalline thin films by controlled atmosphere, low temperature annealing drives ordering through surface energy reduction to an equilibrium structure composed predominately of wide, atomically flat (111) ter-

races, as evidenced through both their electrochemical signature and surface structure determined by scanning tunneling microscopy (STM). Using single component metal and alloy thin films as a template, it is possible to tune the composition, compositional profile and surface structure through thermally induced segregation and ordering, providing valuable insight into the correlation between structure/composition and functional electrocatalytic properties. This insight will help to guide the transition from extended bulk surfaces to nanoscale systems for the development of the next generation of practical electrocatalysts.

EXPERIMENTAL

Thin films were prepared by magnetron sputter deposition onto glassy carbon (GC) disks (6 mm dia., 4 mm thick) in a sputter deposition chamber (AJA International, Inc.) equipped with both radio frequency (RF) and direct current (DC) power supplies and operating with a base pressure of 10^{-10} torr and a sputtering pressure of 1.5 mtorr. Prior to deposition of the metal films, the GC substrates were cleaned with an RF Ar plasma. The Pt films were deposited onto a room temperature GC substrate with 100 W RF power, yielding a rate of 0.75 Å s^{-1}, while the Au films were deposited with 50 W DC power, yielding a rate of 0.74 Å s^{-1}. Both the Pt and Au films were between 10 and 25 nm thick as determined by a quartz crystal thickness monitor. The as-deposited films were annealed in a tube furnace under a controlled atmosphere, 3 % H_2/Ar at 500 °C for Pt and 300 °C for Au.

The nanostructured thin film catalysts (NSTF) were formed through magnetron sputter deposition of platinum and platinum alloys onto the surface of an oriented, crystalline organic pigment (*N*,*N*-di(3,5-xylyl)perylene-3,4:9,10bis(dicarboximide), Perylene Red) whiskers.[30] Structural ordering of the NSTF was achieved through thermal annealing at 400 °C in a H_2/Ar atmosphere.

A typical three-compartment, Pyrex electrochemical cell was used for all electrochemical measurements, in which the SCE (Hg/HgCl, Beckman) reference electrode was separated from the working electrode compartment by a salt bridge and the Pt counter electrode was separated with a porous glass frit. All potentials in this study are reported *versus* the reversible hydrogen electrode (RHE). The thin, sputtered/annealed films on GC disks were characterized electrochemically in the hanging meniscus configuration in Ar-purged 0.1 M $HClO_4$ and 0.1 M H_2SO_4 electrolytes, which were made from high purity acids. The thin films were immersed in the electrolyte under potential control (0.1 V *vs*. RHE).

The scanning tunneling microscopy (STM) images for the Pt-thin films were acquired with a Digital Instruments Multi-Mode Dimension STM controlled by a Nanoscope III control station. During the measurement, the microscope and sample were enclosed in a pressurized cylinder with a CO atmosphere. Prior to the introduction of the sample into the STM, a CO layer was adsorbed onto the surface in CO saturated 0.1 M $HClO_4$, to both preserve the order and cleanliness of the surface and to aid in the visualization of the surface atomic structure with respect to the formation of an ordered CO adlayer. STM images of the Au and Pt-thin films were also recorded in an Omicron UHV system equipped with an STM chamber. Samples were imaged at 0.20 V and 1.0 nA.

A Hitachi H-9500 environmental transmission electron microscope operated at 300 kV was used to perform microstructural characterization and the *in situ* heating TEM study. Powder samples were attached to the heating zone of a Hitachi gas injection–heating holder. Images of the nanoparticles were first recorded at room temperature, followed by heating of

the specimen inside the microscope chamber with a vacuum level of about 10^{-4} Pa. A CCD (charged-couple device) camera was used to monitor the microstructural evolution and record images and videos. Each heating temperature was held for at least 10 min for detailed structural characterization, including morphology and atomic structure. A Hitachi SU70 high-resolution field-emission SEM was used for routine inspection of NSTF samples. For a detailed study of the surface morphology study at nanometer scale, a Hitachi S-5500 ultrahigh resolution cold field-emission SEM delivered a much higher resolution power (0.4 nm secondary electron image resolution at 30 kV) than normal SEM because of the specially designed objective lens. On both SU70 and S-5500, secondary electron images were taken at 15 or 30 kV to reveal the surface morphology of both the as-deposited and annealed samples.

RESULTS AND DISCUSSIONS

Magnetron sputter deposition is well suited for the efficient growth of thin single component, layered and well-mixed alloy films. The surface morphology of the as-sputtered thin films, however, is typically three-dimensional (3D) with grain sizes averaging 5 nm, Figs. 1a and 2a. Consequently, their electrochemical behavior is typical of bulk polycrystalline materials, Figs. 1a and 2a. The extent of this 3D morphology and surface roughness can be limited through optimization of the sputtering parameters, where lower sputter gas pressures will limit gas incorporation into the films and maintain the high kinetic energy of the impinging atoms. High kinetic energy impingement facilitates the formation of dense films with an absence of columnar grains, which may limit grain growth during annealing, and produce a film with predominately (111) orientation of the individual grains.[31,32] For FCC metals; however, the surface orientations of these small grains are not necessarily (111).

Annealing thin films in a reductive atmosphere facilitates surface diffusion, which tends to smoothen defects and promote growth of the lowest energy (111) facets. This process is promoted by the use of an amorphous substrate as the film is not epitaxially constrained to the crystallographic structure of the underlying substrate, and hence, surface diffusion and grain boundary motion are sufficiently fast at moderate annealing temperatures to induce coalescence and growth of grains. Evolution of film discontinuities, holes, hillocks,[33–35] grain boundary grooves[36] and film dewetting,[37] can cause films to roughen during annealing. These processes become exacerbated as both film thickness and melting point of the metal decrease. Therefore, care must be taken when annealing thin, sputtered films to balance effectively the competitive atomic processes of smoothening driven by surface energy reduction and roughening through formation of film discontinuities. Roughening can be avoided by using moderate annealing temperatures, ≈0.3 T_m (melting point), above which, film dewetting and incorporation of carbon impurities are evidenced by the loss of the characteristic (111) features in the CVs. These lower temperatures prove to be sufficient to induce surface diffusion driven structural ordering in the thin films. When comparing the CV signatures of as-sputtered and annealed Pt-thin films to that of a Pt(111) single

crystal, Fig. 1a, c and d, the dramatic transition from polycrystalline to a highly ordered surface becomes apparent. The as-sputtered Pt-thin film has an electrochemical signature resembling that of a polycrystalline Pt-electrode with hydrogen underpotential deposition (H_{UPD}) peaks associated with proton adsorption on steps and defect sites and broad oxidation/reduction features at higher potentials, consistent with the small grained, atomically rough structure of the film. The surface of the annealed Pt-thin film, on the other hand, is characterized by a well ordered morphology containing large, interconnected, atomically flat terraces, as shown by the hexagonal (2×2)–3CO adstructure of the CO_{ad} layer on Pt in the STM image in Fig. 1b; an adsorbate structure that only occurs on atomically ordered (111) terraces.[38]

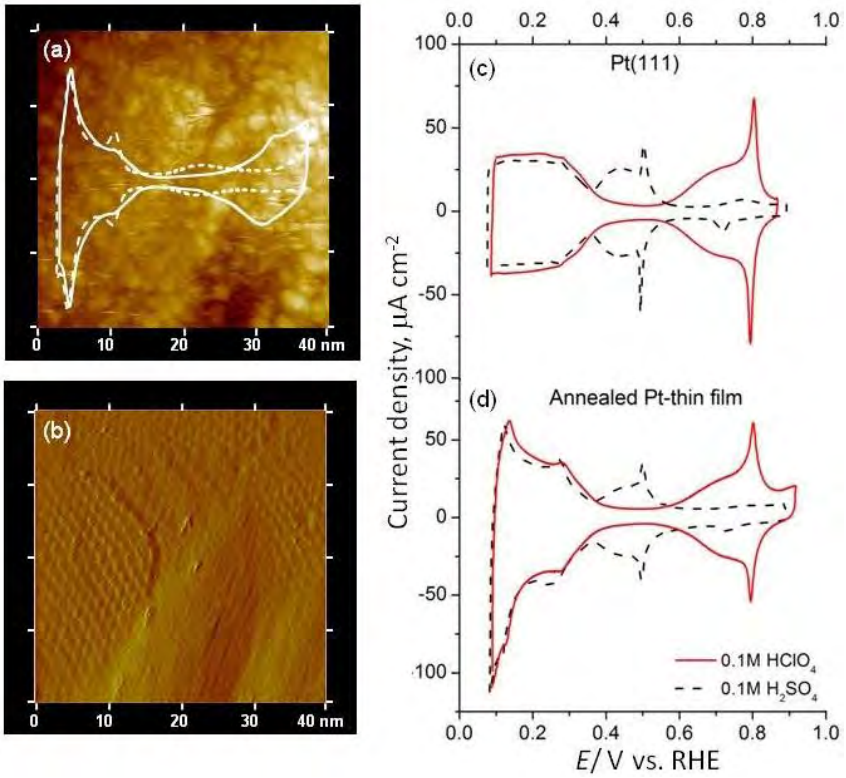

Fig. 1. Scanning tunneling microscopy (STM) images of: a) as-sputtered Pt-thin film and b) a CO_{ad} layer on an annealed Pt-thin film on a GC substrate. The hexagonal structures shown in (b) are attributed to an ordered CO_{ad} layer that is only visible on clean, atomically flat (111) terraces. The overlying CVs in (a) represent the electrochemical signature of the as-sputtered Pt films in 0.1 M $HClO_4$ (solid line) and 0.1 M H_2SO_4 (dashed line). c) CVs of Pt(111) in 0.1 M $HClO_4$ (red line) and 0.1 M H_2SO_4 (dashed black line); d) CVs of an annealed Pt-thin film in 0.1 M $HClO_4$ (red line) and 0.1 M H_2SO_4 (dashed black line). All electrolytes were purged with Ar and the CVs were recorded at a sweep rate of 50 mV s^{-1}.

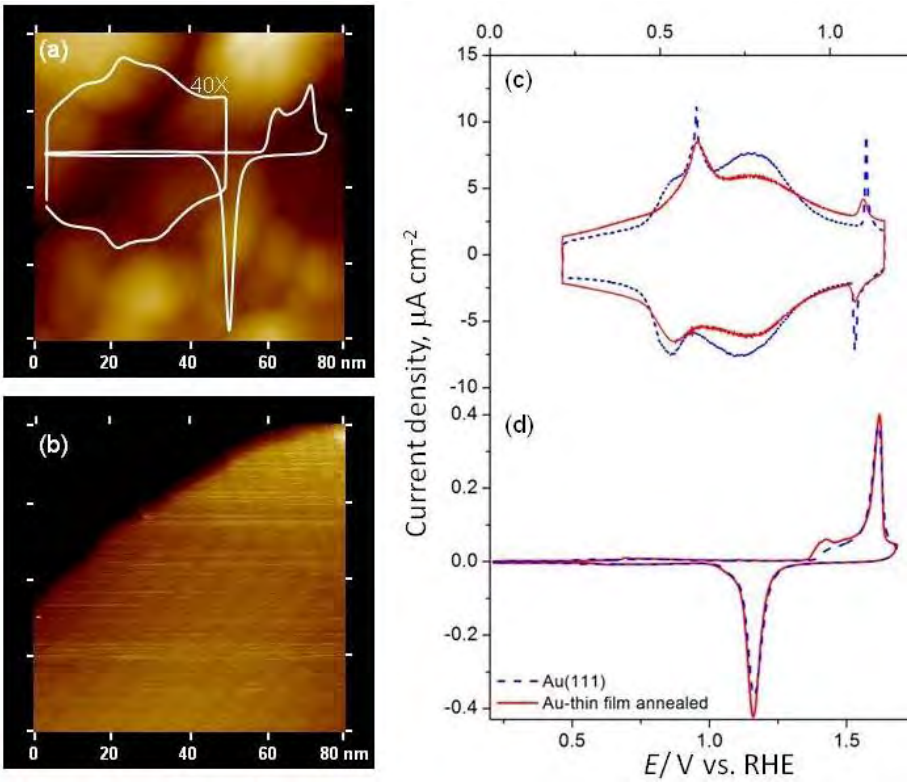

Fig. 2. Scanning tunneling microscopy (STM) images recorded in UHV (100 nm×100 nm), 0.20 V and 1.0 nA, of: a) an as-sputtered Au-thin film, overlain with the CV of the as-sputtered Au-thin film in 0.1 M H_2SO_4, including an expanded current signal for the low potential region and b) an atomically flat Au(111) terrace on an annealed, sputtered Au-thin film on a GC disk substrate. The herringbone $(\sqrt{3}\times 23)$ reconstruction is clearly visible and the terrace width of over 50 nm was routinely found over the entire surface of the annealed Au-thin films. c) CVs of the low potential region for Au(111) (blue dashed line) and annealed Au-thin film (red line); d) CVs including the Au oxidation region for Au(111) (blue dashed line) and annealed Au-thin film (red line) recorded in room temperature, Ar purged 0.1 M H_2SO_4 at a sweep rate of 50 mV s^{-1}.

Characteristic electrochemical features of Pt(111) appeared for the annealed Pt-thin films in both $HClO_4$ and H_2SO_4 electrolytes, Fig. 1c and d. The most telling feature for Pt(111) in $HClO_4$, Fig. 1c, is the sharp, reversible butterfly peak at ≈0.8 V *vs*. RHE, which is attributed to adsorption/desorption of OH_{ad} species and its peak current and sharpness is a descriptive metric for both the cleanliness and crystalline order of the surface.[39–42] It is a feature that, while absent for the as-sputtered Pt-thin film, Fig. 1a, iss as sharp and similar in peak current density for the annealed Pt-thin film as for a Pt(111) electrode, which is indicative of long-range ordering associated with large, interconnected (111) terraces present

on the annealed thin film, Fig. 1d. Voltammetric observation of the adsorption of anionic species other than hydroxyl can give further insight into the state of the annealed Pt-thin film surface. In 0.1 M H_2SO_4 electrolyte, Fig. 1c, a butterfly peak appears at ≈0.5 V *vs*. RHE for Pt(111), although the exact position is dependent on the HSO_4^- concentration in solution.[13,43] This reversible feature is attributed to the order/disorder transition of a long-range disordered sulfate layer, the adsorption of which is represented by the current hump preceding the butterfly peak.[43–46] The presence and sharpness of this peak is strongly tied to the defect density of the surface, whereby this feature is not observed even for evaporated[17] or electrodeposited[26] Pt-thin films on single crystal substrates. The potential, sharpness and peak intensity of this butterfly feature may be associated with surface structures by studying the response of different miscut angles, vicinal surfaces, of a (111) single crystal. As the terrace width decreases and the step/ /defect density increases, the peak intensity decreases and eventually disappears.[13,14] The minimum average terrace width for the studied annealed Pt-thin films may be estimated by comparing the CV in 0.1 M H_2SO_4, Fig. 1d, to those of a series of miss-cut Pt(111) single crystals. It is found that the finger-print features of the annealed Pt-thin films closely match those of a (13,13,12) surface.[13] The sulfate adsorption butterfly feature in low concentration H_2SO_4 electrolytes (≤0.1 M) disappears for surfaces with an average terrace width below 12 atoms, but only under extremely clean conditions.[13,14] It is not uncommon for the butterfly peak to be poorly resolved in H_2SO_4 for surfaces with terrace widths between 20 and 40 atoms.[13] It can be inferred from the electrochemical results, as they represent an average over the entire surface that the atomic structure of the annealed Pt-thin films is characterized by a minimum average terrace width of at least 15–20 atoms. However, locally, as determined by CO_{ad} STM, Fig. 1b, the annealed Pt-thin film surface contains many areas composed of large, atomically flat terraces with widths greater than 20 nm.

To demonstrate the general applicability of the proposed approach, the presented procedure is extended to the formation of ordered thin films of other electrochemically relevant metals. The CVs of Au(111) and annealed Au-thin films on GC in 0.1 M H_2SO_4 are compared in Fig. 2c and d. The electrochemical signature in the low potential region, ≈0.2 to 1.2 V *vs*. RHE, in H_2SO_4, Fig. 2c, exhibits features characteristic of the (111) crystallographic orientation. The sharp peak in the anodic scan at ≈0.6 V *vs*. RHE is attributed to the lifting of the reconstruction of the Au(111) surface, moving from a $(\sqrt{3}\times 23)$ to a (1×1) structure,[47–51] which is reformed upon reversal of the potential, as evidenced by the hump at ≈0.55 V *vs*. RHE; the asymmetry of the current feature is due to the slow kinetics of the lifting/formation of the reconstruction.[52] After gentle annealing, the rough, small grained morphology of the as-sputtered Au-thin film, for which there are no reconstruction peaks, Fig. 2a, exhibits a clear, well-ordered

structure, as evidenced by the presence of the reconstruction lifting/formation peaks, Fig. 2c, and the visualization of the $(\sqrt{3}\times 23)$ herringbone surface feature through UHV STM, Fig. 2b. Using STM to examine the atomic structure of different areas of the annealed Au-thin film, atomically flat terraces with widths of 50 to 100 nm are found to be ubiquitous across the entire surface.

The lifting of the reconstruction is accompanied by the adsorption of a disordered adlayer of sulfate onto the (111) terrace,[49,51] represented by the broad hump between 0.65 and 1 V *vs*. RHE, Fig. 2c. As the potential is swept anodically, the disordered sulfate adlayer undergoes an order/disorder transition, to which the sharp, reversible "butterfly" peaks at ≈1.1 V *vs*. RHE, Fig. 2c, are attributed.[47–52] The butterfly feature in H_2SO_4 is associated with the long-range order of the surface and disappears for Au(111) single crystals with miscut angles greater than 4° or terrace widths below 3 nm.[15,16,53,54] On expanding the potential range into the Au oxidation/reduction region, peaks associated with the formation of AuOH at ≈1.4 V *vs*. RHE and AuO at ≈1.6 V *vs*. RHE. $Au–OH_{ad}$ tends to adsorb preferentially at step edges and defect sites;[55–57] therefore, the reduction in the size of the peak at ≈1.3 V *vs*. RHE upon annealing to the point where it nearly matches the current of the corresponding feature of the Au(111) CV in conjunction with an increase in the peak current and sharpness of the AuO peak at ≈1.6 V *vs*. RHE are additional indications of the low step edge density associated with the growth in size and population of atomically flat (111) features.[16]

The structural evolution of the surface of sputtered Pt and Au films, two metals with differing materials properties such as melting point, degree of substrate wetting and surface energy, during annealing from a rough, nano-grained surface to one that is highly ordered and consisting of a large proportion of atomically flat (111) terraces demonstrates the general applicability of the presented approach. The insight gained from these thin films opens a unique avenue for tailoring the functional properties of materials with high surface area, *i.e*., thin film-based electrocatalysts relevant to renewable energy-based technologies. It is serendipitous that the lowest energy surface, (111), to which these thin films revert during annealing is also the most active crystallographic orientation for the oxygen reduction reaction (ORR) on Pt-transition metal alloys. Bridging the gap between these extended, well-ordered surfaces and high surface area, nanoscale systems will facilitate the development of electrocatalysts with both superior activity and optimized precious metal utilization. To this end, a thin film-based, high surface area electrocatalyst architecture, known as nanostructured thin films (NSTF), has been created through sputter deposition of Pt and Pt alloys onto the surface of an ordered array of molecular solid whiskers, composed of an organic pigment *N*,*N*-di(3,5-xylyl)perylene-3,4:9,10-bis(dicarboximide), commonly known as Perylene Red.[58–63]

The morphology of these as-sputtered whiskers is shown in Fig. 3a–c, where each whisker is approximately 800–1000 nm in length and the film thicknesses range from 10–20 nm. Close examination of the surface structure of these whiskers, Fig. 3a and c, indicate a corrugated surface structure composed of "whiskerettes" with a high nanoscale roughness and defect density. The surface of these as-sputtered whiskers is easily correlated to that of the as-sputtered Au and Pt-thin film surfaces, where a rough, nano-grained morphology dominates. Optimization of this surface structure can be achieved through application of the presented experimental approach derived for extended thin films. Figure 3d–f presents *in-situ* transmission electron microscopy images (TEM) of NSTF whiskers that have been annealed up to 400 °C under vacuum. These TEMs demonstrate the structural transition of the surface of the NSTF whiskers from a densely corrugated, highly defected, 3D surface to one that is smooth, homogeneous and two-dimensional. This transition is thermodynamically driven, as the enhanced mobility of the surface atoms, imparted by the high temperature, tends to move the surface toward the lowest energy configuration. Grain growth and surface faceting, similar to that seen with the sputtered thin films on GC substrates, are confirmed through the *in-situ* TEM images. Fig. 3d–f, where a (111) texture

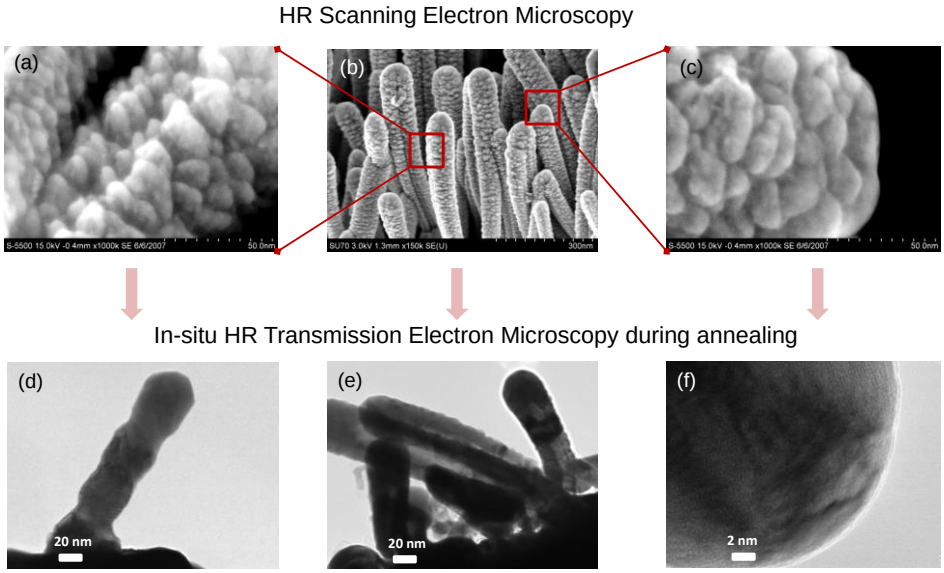

Fig. 3. *In-situ* imaging of the structural transition from nanostructured, 3D to crystalline homogeneous 2D thin films during annealing: a–c) high-resolution scanning electron microscopy (HRSEM) images of the as-sputtered NSTF catalyst; d–f) high resolution transmission electron microscopy (HRTEM) images of the annealed whiskers showing a smooth, faceted surface without corrugated, highly defected whiskerettes.

ordered, (111)-like structure, the controlled annealing atmosphere facilitates the formation of an optimized compositional profile for Pt-transition metal alloys, where the nano-segregated structure mimics that of an annealed $Pt_3Ni(111)$ single crystal.[9] Adsorption characteristics of the oxygenated species are optimized on these Pt segregated surfaces as the high composition of transition metal (Ni, Fe, Co, etc.), greater than the bulk composition of the alloy, in the second atomic layer, changes the electronic structure of the surface Pt atoms, affecting oxygen adsorption strength thereby resulting in improved ORR rates. This change in adsorption properties is evidenced by the CVs shown in Fig. 4a. In the hydrogen underpotential deposition region (H_{UPD}), ≈0 to 0.4 V *vs*. RHE, the signature for the annealed PtNiFe NSTF is a flat plateau that is characteristic of hydrogen adsorption on Pt(111), see Fig. 1c, and Pt alloys,[5,9] whereas that of the as-sputtered Pt and PtNiFe NSTF contain features that may be attributed to H_{UPD} on (100) and (110) surface sites. There is also a positive shift in the onset of surface oxide formation in the order: Pt NSTF < PtNiFe NSTF < annealed PtNiFe NSTF. This shift is indicative of a significant decrease in the surface coverage of hydroxyl species, which can block the active sites for the ORR, and as shown in Fig. 4b and c, results in a significant increase in the ORR activity.

The specific activity is a fundamental property of a material that is indicative of its intrinsic catalytic activity. A higher specific activity is related to an increased turnover frequency due to improved utilization of surface Pt atoms. This improved utilization is a direct result of the ordered surface structure and optimized compositional profile obtained for the annealed PtNiFe NSTF. The ordered PtNiFe NSTF exhibits a specific activity two-times that of the as-sputtered PtNiFe NSTF and nearly 15 times that of commercial Pt/C (TKK) supported nanoparticle electrocatalysts. While film thickness and alloy composition will continue to be optimized, the current annealed PtNiFe NSTF catalyst exceeds the U.S. Department of Energy activity target for 2015 by of a factor of two.

Electrocatalysts are easily categorized by their surface atomic structure and graded by their activity. The low activity class is composed of high surface area supported nanoparticle-based catalysts, followed by polycrystalline alloys and the highest activity class is reserved for single crystal metals. Ordered, annealed Pt alloy NSTF catalysts transcend these classes with activities that are characteristic of single crystal Pt alloys, while maintaining the electrochemically active surface area of nanoscale electrocatalysts. These findings indicate that the ability to tailor atomic structure, composition and morphology could lead to significant enhancements in catalyst activity and precious metal utilization. Through elucidation of the structure–function and composition–function correlations, an approach has been developed in the present study that bridges the gap between extended/bulk surfaces and nanoscale catalysts, providing a new avenue for the design of electrocatalysts with superior functional properties.

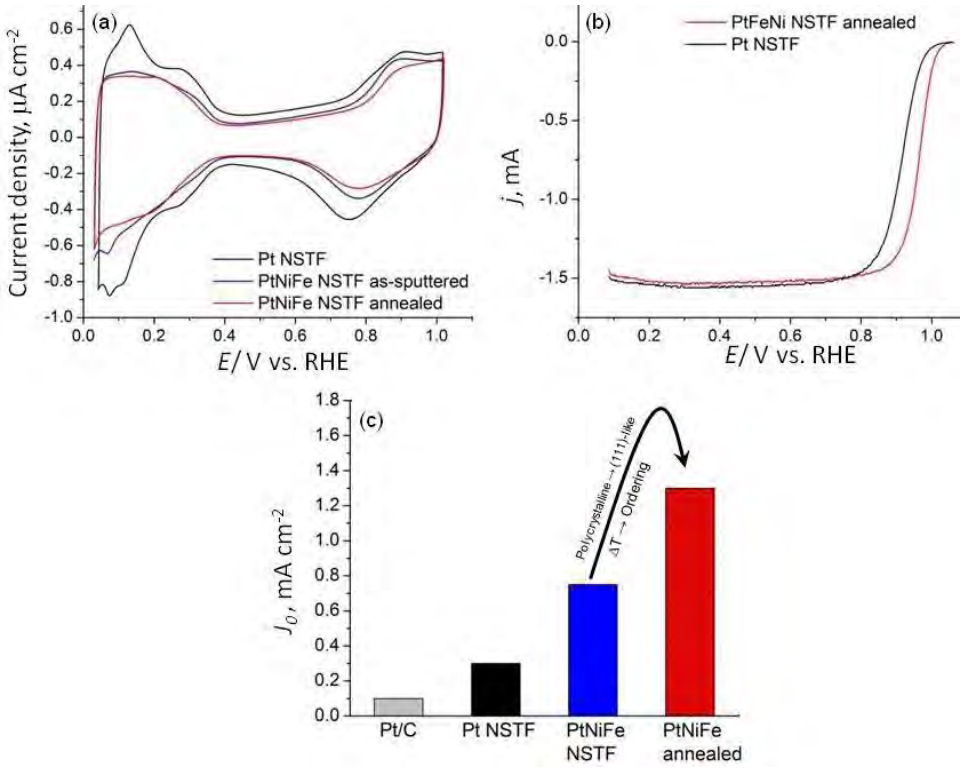

Fig. 4. a) CVs of Pt NSTF (black line), as-sputtered PtNiFe NSTF (blue line) and annealed PtNiFe NSTF (red line) in Ar purged 0.1 M $HClO_4$, recorded with a sweep rate of 50 mV s^{-1}; b) IR-corrected ORR curves for Pt NSTF (black line) and annealed PtNiFe NSTF (red line) in O_2 saturated 0.1 M $HClO_4$, recorded with a sweep rate of 20 mV s^{-1} at room temperature and c) specific activities measured at 0.95 V *vs*. RHE.

CONCLUSIONS

Significant insight into the correlation between structure/composition and functional electrochemical properties has been gained over the years using well-defined single crystal interfaces. Herein, an overview of a generally applicable procedure to reproducibly convert sputtered, polycrystalline thin films on amorphous GC substrates into highly ordered, (111)-like thin films exhibiting the characteristic structural and electrochemical features of carefully prepared (111) single crystal electrodes has been presented. Extension of this approach to practical thin film-based materials allows for the development of a unique class of electrocatalysts that possess the specific activity of bulk/extended surfaces and the electrochemically active surface area of nanoparticle-based catalysts. The superior performance of the annealed PtNiFe thin films, which has a kinetic activity nearly 15 times that of Pt/C, is the direct result of the highly ordered, (111) crystallinity and near-surface compositional profile that develops during

annealing. This approach could facilitate the development of a wide range of practical thin film-based catalysts, bridging the gap between extended/bulk surfaces and nanoscale electrocatalysts.

Acknowledgements. This work was supported by the U.S. Department of Energy, Office of Science, Office of Basic Energy Sciences, under Contract No. DE-AC02-06CH11357. The authors are grateful to Dusan Tripkovic and Arvydas Paulikas (ANL) for support in experimental results obtained by STM, Mark Debe, Radoslav Atanasoski and Dennis van der Vliet (all from 3M) for providing the NSTF catalysts and support in the electrochemical characterizations.

ИЗВОД

ТАНКИ ФИЛМОВИ МОНОКРИСТАЛНЕ СТРУКТУРЕ КАО НОВА КЛАСА ЕЛЕКТРОКАТАЛИЗАТОРА

JOSHUA SNYDER, NENAD M. MARKOVIC и VOJISLAV R. STAMENKOVIC

Materials Science Division, Argonne National Laboratory, Argonne, IL 60439, USA

Широко коришћење монокристалних металних електрода омогућило је значајан увид у везу између атомске структуре површине и функционалних електрохемијских својстава. Међутим, осетљивост њиховог електрохемијског одзива на оријентацију површине и захтевану количину драгоцених метала може да ограничи њихову примену. Овде је изложен опште применљив поступак за добијање танких металних филмова са великим уделом атомски равних тераса оријентације (111) без коришћења епитаксијалне матрице. Термичко одгревање у контролисаној атмосфери танког филма који је магнетронски нанет на аморфну подлогу доводи до његовог уређивања по типу дугог домета. Уређивање оваквих танких металних филмова даје карактеристично електрохемијско обележје површине оријентације (111) уз утрошак минималне количине материјала и обезбеђује адекватну замену за монокристале оријентисане у маси. Овај поступак може да се генерализује за добијање нове класе практичних електрокатализатора заснованих на мултиметалном танком филму код којих је могуће подешавање састава уз површину и морфологије. Одгревање атомски таласастог танког филма Pt-легуре даје високо кристалиничну атомски глатку структуру уређену слично равни (111), чија је површина услед сегрегације обогаћена платином. Она показује супериорна функционална својства, премошћавајући јаз између макроскопских материјала развијених површина и нано-честичних система.

(Примљено 16. септембра, ревидирано 30. октобра 2013)

REFERENCES

1. N. Markovic, H. Gasteiger, P. Ross, *J. Phys. Chem.* **99** (1995) 3411
2. N. Markovic, T. Schmidt, V. Stamenkovic, P. Ross, *Fuel Cells* **1** (2001) 105
3. N. Markovic, R. Adzic, B. Cahan, E. Yeager *J. Electroanal. Chem.* **377** (1994) 249
4. M. Macia,, E. Herrero, J. Feliu, *J. Electroanal. Chem.* 564 (2004) 141
5. D. van der Vliet, C. Wang, D. Tripkovic, D. Strmcnik, X. Zhang, M. Debe, R. Atanasoski, N. Markovic, V. Stamenkovic, *Nat. Mater.* **11** (2012) 1051
6. N. Markovic, H. Gasteiger, P. Ross, *J. Electrochem. Soc.* **144** (1997) 1591
7. J. Greely, J. Rossmeisl, A. Hellman, J. Norskov, *Z. Phys. Chem.* **221** (2007) 1209
8. V. Climent, J. Feliu, *J. Solid State Electrochem.* **15** (2011) 1297

9. V. Stamenkovic, B. Fowler, B. B. Mun, G. Wang, P. Ross, P. C. Lucas, C. N. Markovic, *Science* **315** (2007) 493
10. J. Clavilier, R. Faure, G. Guinet, R. Durand, *J. Electroanal. Chem.* **107** (1979) 205
11. J. Clavilier, D. Armand, B. Wu, *J. Electroanal. Chem. Interfacial Electrochem.* **135** (1982) 159
12. J. Clavilier, *J. Electroanal. Chem.* **107** (1979) 211
13. J. Clavilier, K. El Achi, A. Rodes, *Chem. Phys.* **141** (1990) 1
14. N. Furuya, S. Koide, *Surf. Sci.* **220** (1989) 18
15. T. Wandlowski, K. Ataka, S. Pronkin, D. Diesing, *Electrochim. Acta* **49** (2004) 1233
16. M. Schneeweiss, D. Kolb, D. Liu, D. Mandler, *Can. J. Chem.* **75** (1997) 1703
17. B. Braunschweig, A. Mitin, W. Daum, *Surf. Sci.* **605** (2011) 1082
18. Y. Golan, L. Margulis, I. Rubinstein, *Surf. Sci.* **264** (1992) 312
19. N. Spiridis, M. Kisielewski, A. Maziewski, T. Slezak, P. Cyganik, J. Korecki, *Surf. Sci.* **507–510** (2002) 546
20. S. Broukhin, C. Saguy, M. Koifman, B. Pokroy, *J. Phys. Chem., C* **116** (2012) 12149
21. D. Trevor, C. Chidsey, D. Loiacono, *Phys. Rev. Lett.* **62** (1989) 929
22. G. Scavia, E. Agostinelli, S. Laureti, G. Varvaro, B. Paci, A. Benerosi, V. Albertini, S. Kaciulis, A. Mezzi, *J. Phys. Chem., B* **110** (2006) 5529
23. M. Debe, *Nature* **486** (2012) 43
24. Y. Yamada, K. Miyamoto, T. Hayashi, Y. Iijima, N. Todoroki, T. Wadayama, *Surf. Sci.* **607** (2013) 54
25. Y. Liu, D. Gokcen, U. Bertocci, T. Moffat, *Science* **338** (2012) 1327
26. K. Uosaki, S. Ye, H. Naohara, Y. Oda, T. Haba, T. Kondo, *J. Phys. Chem., B* **101** (1997) 7566
27. A. Berna, J. Delgado, J. Orts, A. Rodes, J. Feliu, *Langmuir* **22** (2006) 7192
28. A. Maljusch, J. Henry, W. Schuhmann, A. Bondarenko, *Electrochem. Comm.* **16** (2012) 88
29. J. Henry, A. Maljusch, M. Huang, W. Schuhmann, A. Bondarenko, *ACS Catalysis* **2** (2012) 1457
30. M. K. Debe, A. Hester, G. Vernstrom, A. Steinbach, S. Hendricks, A. Schmoeckel, R. Atanasoski, D. McClure, P. Turner, *Nanostructured Thin Film Catalysts for PEM Fuel Cells by Vacuum Web Coating*, in *Society of Vacuum Coaters 50th Annual Technical Conference Proceedings*, 2007, p. 175
31. M. Kawamura, T. Mashima, Y. Abe, K. Sasaki, *Thin Solid Films* **377–378** (2000) 537
32. E. Slavcheva, G. Ganske, G. Topalov, W. Mokwa, U. Schnakenberg, *Appl. Surf. Sci.* **255** (2009) 6479
33. J. Tersoff, F. LeGoues, *Phys. Rev. Lett.* **72** (1994) 3570
34. H. Galinski, T. Ryll, L. Schlagenhauf, L. Gauckler, *Phys. Rev., B* **85** (2012) 125408
35. W. Pennebaker, *J. Appl. Phys.* **40** (1969) 394
36. M. Rost, D. Quist, J. Frenken, *Phys. Rev. Lett.* **91** (*2003*) 026101
37. S.-J. Hwang, J.-H. Jee, C.-O. Jeong, Y.-C. Joo, *Scripta Mat.* **56** (2007) 17
38. D. Strmcnik, D. Tripkovic, D. van der Vliet, K. Chang, V. Komanicky, H. You, G. Karapetrov, J. Greeley, V. Stamenkovic, N. Markovic, *J. Am. Chem. Soc.* **130** (2008) 15332
39. A. Bondarenko, I. Stephens, H. Hansen, F. Perez-Alonso, V. Tripovic, T. Johansson, J. Rossmeisl, J. Norskov, I. Chorkendorff, *Langmuir* **27** (2011) 2058
40. A. Berna, V. Climent, J. Feliu, *Electrochem. Comm.* **9** (2007) 2789
41. E. Herrero, J. Feliu, A. Wieckowski, J. Clavilier, *Surf. Sci.* **325** (1995) 131

42. N. Markovic, T. Schmidt, B. Grgur, H. Gasteiger, R. Behm, P. Ross, *J. Phys. Chem., B* **103** (1999) 8568
43. N. Garcia-Araez, V. Climent, P. Rodriguez, J. Feliu, *Electrochim. Acta* **53** (2008) 6793
44. M. Koper, J. Lukkien, *J. Electroanal. Chem.* **485** (2000) 161
45. B. Braunschweig, W. Daum, *Langmuir* **25** (2009) 11112
46. A. Funtikov, U. Stimming, R. Vogel, *J. Electroanal. Chem.* **428** (1997) 147
47. M. Schneeweiss, D. Kolb, *Solid State Ionics* **94** (1997) 171
48. K. Sato, S. Yoshimoto, J. Inukai, K. Itaya, *Electrochem. Comm.* **8** (2006) 725
49. O. Magnussen, J. Hagebock, J. Hotlos, R. Behm, *Faraday Discuss.* **94** (1992) 329
50. F. Silva, A. Martins, *Electrochim. Acta* ***44*** (1998) 919
51. T. Kondo, J. Morita, K. Hanaoka, S. Takakusagi, K. Tamura, M. Takahasi, J. Mizuki, K. Uosaki, *J. Phys. Chem., C* **111** (2007) 13197
52. Z. Shi, J. Lipkowski, S. Mirwald, B. Pettinger, *J. Electroanal. Chem.* **396** (1995) 115
53. A. Cuesta, M . Kleinert, D. Kolb, *Phys. Chem. Chem. Phys.* **2** (2000) 5684
54. M. Holzle, V. Zwing, D. Kolb, *Electrochim. Acta* **40** (1995) 1237
55. C. Vitus, A. Davenport, *J. Electrochem. Soc.* **141** (1994) 1291
56. H. Hondo, S. Sugawara, K. Itaya, *Anal. Chem.* **62** (1990) 2424
57. A. Hamelin, *J. Electroanal. Chem.* **407** (1996) 1
58. D. van der Vliet C. Wang, M. Debe, R. Atanasoski, N. M. Markovic, V. R. Stamenkovic, *Electrochim. Acta* **56** (2011) 8695
59. M. K. Debe, A. R. Drube, *J. Vac. Sci. Technol., B* **13** (1995) 1236
60. M. K. Debe, R. J. Poirier, *J. Vac. Sci. Technol., A* **12** (1994) 2017
61. M. K. Debe, A. K. Schmoeckel, G. D. Vernstrom, R. Atanasoski, *J. Power Sources* **161** (2006) 1002
62. L. Gancs, T. Kobayashi, M. K. Debe, R. Atanasoski, A. Wieckowski, *Chem. Mater.* ***20*** (2008) 2444
63. M. K. Debe, *J. Electrochem Soc.* **160** (2013) F522.